American Mineralogist, Volume 78, pages 345–359, 1993

Influences of reaction history and chemical diffusion on *P-T* calculations for staurolite schists from the Littleton Formation, northwestern New Hampshire

FRANK P. FLORENCE,* FRANK S. SPEAR
Department of Earth and Environmental Sciences, Rensselaer Polytechnic Institute, Troy, New York 12180, U.S.A.

ABSTRACT

Geothermometry from staurolite-grade pelitic assemblages may fail to reflect peak temperatures of metamorphism because of (1) prograde garnet-consuming reactions, and (2) diffusional reequilibration during cooling in response to retrograde reactions. Garnet dissolution during staurolite formation leads to sharp compositional gradients within a few micrometers of garnet rims. These gradients may then be modified by diffusion on cooling and lead to anomalous temperature estimates calculated from thermobarometers involving garnet.

Numerical simulations of mineral growth and diffusion were used to examine these effects for a prograde metamorphic sequence from the Salmon Hole Brook syncline, northwestern New Hampshire. In higher grade assemblages, mineral textures indicate that staurolite grew by the consumption of garnet, and garnet-biotite temperature estimates fall in the range 515 ± 30 °C. Interbedded layers containing garnet and biotite, but not staurolite, yield temperature estimates of 565 ± 25 °C. In the eastern portion of the syncline, rocks containing kyanite + staurolite + garnet + biotite assemblages indicate temperatures of 550 ± 25 °C. Hypothetical growth and reaction histories that adhere to the modal, mineralogical, and known geochronological constraints were developed using a thermodynamically rigorous treatment of mineral modes and compositions incorporating calculations for multicomponent diffusion in garnet. These models demonstrate that temperature estimates from staurolite schists may underestimate actual thermal maxima by more than 50 °C. Garnet growth accompanying the reaction staurolite = kyanite + biotite + garnet can lead to higher absolute temperature estimates, but these may still be at least 50 °C lower than actual peak temperatures. Simulations also demonstrate that Fe enrichment in biotite accompanying retrograde production of chlorite may lead to calculated temperatures that are 10–50 °C higher than would occur where only diffusional exchange operated on cooling. Evidence from additional metamorphic terranes suggests that this reaction model has wide applicability.

INTRODUCTION

Phase relations in garnet-grade metapelites are often sufficiently comprehensible to allow characterization of the pressure-temperature (*P-T*) conditions of equilibration. At higher grades, however, determination of the *P-T* conditions of metamorphism may not be straightforward. Mineral compositions may reflect both prograde and retrograde reactions that can lead to erroneous variations in calculated pressures and temperatures. In the case of staurolite-bearing assemblages, compositional zoning in garnet can be modified as the result of an interval of consumption along a prograde reaction sequence and by postgrowth volume diffusion.

The objective of this report is to clarify whether thermobarometry estimates for staurolite-bearing samples actually reflect *P-T* conditions at the highest grade of metamorphism by examining the metamorphism of amphibolite-grade pelitic rocks associated with the Salmon Hole Brook syncline in northwestern New Hampshire. Temperature estimates from this region fail to conform to the apparent sequence of prograde metamorphism deduced from mineral assemblages, i.e., higher temperature estimates were obtained from garnet + biotite + chlorite assemblages than from kyanite + staurolite + garnet + biotite assemblages. A combination of causes is believed to be responsible for this behavior. First, variations in net-transfer reaction histories experienced by different metapelitic samples can lead to significant differences in the amount of chemical information that is preserved in minerals (Spear et al., 1990). As well, thermobarometry estimates and *P-T* path calculations from staurolite-grade metapelites may be influenced by chemical relaxation of zoning and reequilibration during cooling (Florence and Spear, 1991; Spear, 1991). We report here on forward models that consider both the effects of net-transfer and exchange reactions and diffusional reequilibration along

* Present address: Department of Geology, Syracuse University, Syracuse, New York 13244, U.S.A.

0003–004X/93/0304–0345$02.00

a combined prograde and retrograde *P-T-t* path. Our findings confirm that, in staurolite-grade metapelites, special attention needs to be given to the correct identification of the reactions responsible for the growth and consumption of chemically zoned phases such as garnet and plagioclase and stress the need to determine the extent that diffusion may have modified initial (growth) chemical zoning.

Analytical methods

Mineral compositions were measured from prepared petrographic sections using wavelength-dispersive methods on an automated Jeol 733 electron microprobe at Rensselaer Polytechnic Institute. Operating conditions were 15 Kv accelerating potential, a sample current of 10–25 nA, and a beam diameter of 2–10 μm. Natural minerals were used as analytical standards, and calibrations were verified on secondary standards. Data reduction followed the procedure of Bence and Albee (1968), with the correction factors of Albee and Ray (1970). All measured Fe is reported as Fe^{2+}.

Mineral compositions are presented in Table 1. Rim to core line scans of multiple analyses were used to obtain detailed compositional information from zoned minerals, particularly plagioclase and garnet. Analyses were obtained at a 2-μm spacing over the first 50 and a 5-μm spacing for the next 150 μm. Wider spacing of 10 and 25 μm were used to 0.5 and 1.0 mm, respectively. Efforts were made to obtain mineral compositions from each sample that reflect maximum temperature conditions. Matrix phase compositions were obtained from grains within a few hundred micrometers of the reported garnet composition. Multiple grains of biotite, muscovite, and chlorite were analyzed to test for compositional homogeneity. Plagioclase typically was zoned outwardly to lower X_{an}, and reported compositions are from rims. Garnet compositions without exception showed a pattern of decreasing Fe/(Fe + Mg) toward the rim. Many garnets also showed upturns in this ratio within 100 μm or less of the rim that probably reflect modification of original growth zoning by diffusion during cooling. Tabulated garnet compositions are near-rim analyses coincident with the minimum Fe/(Fe + Mg) ratio.

Metamorphism, thermobarometry, and *P-T* paths

The Salmon Hole Brook syncline is part of a tightly folded synclinal belt that lies along the western flank of the Bronson Hill anticlinorium in western New Hampshire (Fig. 1). These structures were produced during the early Devonian Acadian orogeny and have been described by Billings (1937) and Rumble (1969). Toward the northern end of the belt, the Haverhill Pluton of the Bethlehem Gneiss separates a northern syncline cored by the Lower Devonian Littleton Formation from a narrow syncline that extends southward. For simplicity, the name Salmon Hole Brook syncline, originally applied to the western portion of the northern syncline by Billings, is used here to signify the entire northern syncline.

The timing of regional metamorphism in northwestern New Hampshire is broadly constrained to have occurred between intrusion of the Bethlehem granodiorite gneiss, represented in the study area by the Mount Clough and Haverhill Plutons, and isotopic closure temperatures for metamorphic minerals. The Mount Clough Pluton has been dated at 410 ± 5 Ma (Moench and Aleinikoff, 1991, U-Pb zircon). A U-Pb age of 392 ± 8 Ma from monazite in sillimanite-grade metasediments to the east of the Bronson Hill anticlinorium (Barreiro and Eusden, 1988) may date the approximate peak of thermal events in the region. Cooling ages from hornblende, biotite, and muscovite (Spear and Harrison, 1989; Harrison et al., 1989) obtained immediately south of the Salmon Hole Brook area show that cooling had progressed to below 500 °C by 310 Ma and to about 300 °C by 250 Ma. On the basis of this cooling history, it is likely that closure temperatures for retrograde exchange reactions were reached between approximately 350 and 300 Ma.

The regional isograd pattern around the Salmon Hole Brook syncline (Florence, 1991) reflects an overall increasing grade of metamorphism from west to east (Fig. 2). Chlorite and biotite grade rocks occur in a narrow zone within a few kilometers of the Ammonoosuc Fault, a Mesozoic age structure separating exclusively low-grade rocks on the west from higher grade rocks to the east. Further to the east, garnet-grade assemblages are found discontinuously in rocks stratigraphically below the Littleton Formation. Littleton Formation rocks in the Salmon Hole Brook syncline were metamorphosed to kyanite-staurolite grade.

Pelitic rocks of the Littleton Formation contain a number of distinct AFM mineral assemblages (also see Dickenson, 1988). These include (1) garnet + biotite + chlorite, (2) staurolite + garnet + biotite + chlorite, (3) staurolite + garnet + biotite + chlorite + chloritoid, and (4) kyanite + staurolite + garnet + biotite. All assemblages contain coexisting muscovite, quartz, ilmenite, and graphite, and most include plagioclase. Apatite and tourmaline are ubiquitous accessory minerals. The large majority of the rocks examined contained the assemblage staurolite + garnet + biotite + chlorite. Assemblage 3, containing chloritoid, was recognized at only one locality within the syncline. Otherwise, chloritoid was not found as either a matrix phase or as inclusions in porphyroblasts. The kyanite-bearing assemblage occurs in rocks in the northeastern portion of the Salmon Hole Brook syncline (Fig. 2), and one sample from there also contains andalusite.

P-T paths of metamorphism have been calculated from the Salmon Hole Brook syncline (Florence, 1991) using the Gibbs method of differential thermobarometry (Spear, 1989) in combination with correlated compositional changes in zoned garnet, plagioclase inclusions, and zoned matrix plagioclase. *P-T* paths calculated from garnet +

TABLE 1. Representative mineral compositions in cations per mineral formula

Chlorite normalized to 28 O atoms									
Sample	8809	8835	8844	8848	8859	8864	8874	8885	8886
Si	5.079	5.276	5.191	5.213	5.142	5.089	5.412	5.109	5.133
Al	5.992	5.536	5.836	5.734	5.810	5.896	5.480	5.869	5.873
Ti	0.017	0.010	0.019	0.019	0.019	0.013	0.014	0.020	0.014
Mg	4.445	3.883	4.538	4.510	4.627	4.718	4.682	4.484	4.693
Fe^{2+}	4.358	5.238	4.276	4.383	4.324	4.217	4.197	4.445	4.167
Mn	0.017	0.002	0.011	0.009	0.012	0.017	0.048	0.004	0.033
Oxide sum	87.33	86.45	88.22	87.99	87.90	87.53	87.37	87.77	87.78
Fe/(Fe + Mg)	0.495	0.574	0.485	0.493	0.483	0.472	0.473	0.498	0.470

Biotite normalized to 11 O atoms											
Sample	8809	8835	8844	8848	8859	8864	8866	8874	8885	8886	9047C
Si	2.680	2.712	2.680	2.681	2.688	2.726	2.679	2.753	2.698	2.721	2.755
Al	1.773	1.780	1.776	1.812	1.803	1.745	1.763	1.714	1.767	1.728	1.699
Ti	0.084	0.107	0.070	0.092	0.078	0.091	0.082	0.101	0.081	0.068	0.090
Mg	1.110	0.863	1.149	0.912	1.165	1.135	1.307	1.058	1.099	1.177	1.209
Fe^{2+}	1.231	1.399	1.241	1.414	1.187	1.172	1.094	1.212	1.238	1.193	1.099
Mn	0.005	0.001	0.000	0.003	0.000	0.005	0.002	0.009	0.005	0.001	0.001
Ca	0.004	0.007	0.004	0.000	0.000	0.001	0.003	0.002	0.001	0.002	0.001
Na	0.026	0.023	0.012	0.048	0.051	0.073	0.017	0.021	0.051	0.072	0.036
K	0.900	0.818	0.837	0.790	0.772	0.794	0.838	0.857	0.831	0.821	0.859
Oxide sum	96.10	94.36	95.23	94.88	94.84	94.51	94.29	94.13	96.04	94.25	94.64
Fe/(Fe + Mg)	0.526	0.618	0.519	0.608	0.505	0.508	0.456	0.534	0.530	0.503	0.476

Garnet normalized to 12 O atoms											
Sample	8809	8835	8844	8848	8859	8864	8866	8874	8885	8886	9047C
Si	2.948	2.964	2.987	2.976	2.991	2.966	2.969	3.066	2.980	2.982	3.012
Al	2.020	2.005	2.039	2.025	2.015	2.032	2.010	1.996	2.042	2.034	1.969
Mg	0.327	0.242	0.313	0.243	0.316	0.332	0.380	0.305	0.302	0.324	0.353
Fe^{2+}	2.430	2.543	2.359	2.610	2.362	2.399	2.093	2.052	2.379	2.241	2.107
Mn	0.193	0.032	0.236	0.022	0.237	0.104	0.384	0.423	0.188	0.330	0.355
Ca	0.125	0.249	0.058	0.137	0.081	0.184	0.188	0.093	0.107	0.090	0.206
Oxide sum	100.41	102.02	101.45	101.97	102.60	100.78	101.81	100.69	101.69	101.59	100.23
Fe/(Fe + Mg)	0.881	0.913	0.883	0.915	0.882	0.878	0.846	0.871	0.887	0.874	0.857

Staurolite normalized to 48 O atoms*									
Sample	8809	8844	8848	8859	8864	8866	8885	8886	9047C
Si	7.610	7.568	7.740	7.773	7.713	7.634	7.646	7.760	7.728
Al	17.938	18.060	17.812	17.653	17.830	17.846	17.952	18.007	17.794
Ti	0.100	0.101	0.082	0.111	0.118	0.138	0.104	0.115	0.135
Mg	0.750	0.737	0.501	0.730	0.727	0.707	0.611	0.684	0.725
Fe^{2+}	3.202	3.228	3.215	3.383	3.328	3.186	3.056	2.835	3.037
Mn	0.037	0.033	0.007	0.050	0.012	0.081	0.033	0.068	0.062
Zn	0.053	0.045	0.285	0.061	0.002	0.083	0.243	0.123	0.131
Oxide sum	98.19	98.42	98.33	98.50	98.09	95.86	99.13	98.09	97.49
Fe/(Fe + Mg)	0.810	0.814	0.865	0.823	0.821	0.832	0.834	0.805	0.807

Plagioclase normalized to eight O atoms											
Sample	8809	8835	8844	8848	8859	8864	8866	8874	8885	8886	9047C
Si	2.807	2.781	2.860	2.842	2.850	2.677	2.669	2.906	2.831	2.812	2.651
Al	1.184	1.198	1.135	1.168	1.142	1.327	1.312	1.114	1.198	1.176	1.340
Ca	0.188	0.293	0.124	0.167	0.151	0.308	0.314	0.105	0.201	0.181	0.362
Na	0.830	0.692	0.904	0.793	0.857	0.688	0.706	0.814	0.668	0.850	0.638
K	0.004	0.002	0.002	0.002	0.002	0.002	0.003	0.004	0.003	0.004	0.005
Oxide sum	100.56	99.64	100.46	99.19	98.43	99.74	100.32	100.28	100.16	100.72	99.40

* Normalization also assumes 3.06 H and 0.2 Li, following the treatment of Holdaway et al. (1986).

biotite + chlorite ± staurolite assemblages consistently indicate that garnet growth initially took place during pressure increases of 800 to >2000 bars with concurrent heating of <20 °C. This steep pressure increase was followed by a heating trend of between 5 and 40 °C, with only limited increase in pressure. These results are consistent with petrographic evidence indicating that prograde metamorphism was ongoing during tectonism and ultimately outlasted deformation (see below). Additional evidence for increasing pressure during metamorphism is given by kyanite-staurolite-garnet-biotite schists from the northeastern portion of the syncline that contain xenoblastic andalusite in the matrix. The andalusite grains overprint an early fabric and are partly replaced by muscovite aligned with the matrix foliation, whereas kyanite blades are randomly oriented with respect to the foliation. These textures suggest that andalusite formed pre- or syntectonically and persisted metastably as kyanite crystallized after deformation had ceased. A minimum pressure increase of 1.0 kbar greater than the aluminum

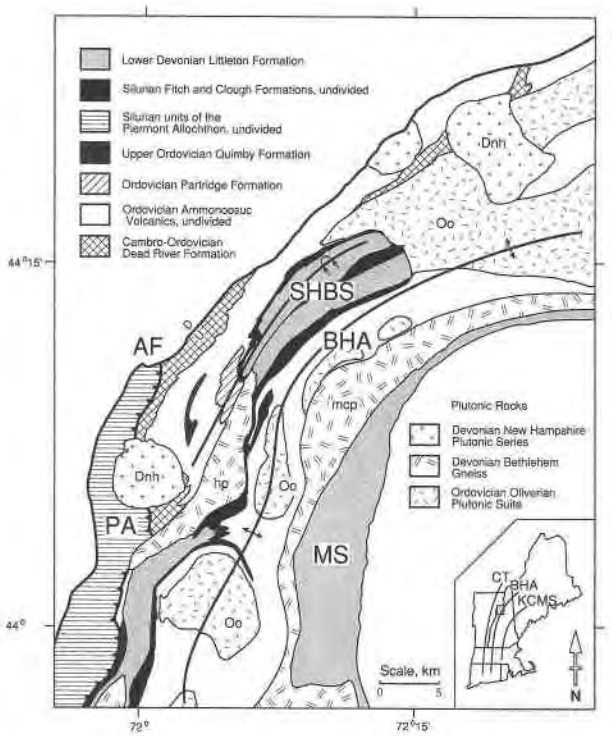

Fig. 1. Generalized geologic map of northwestern New Hampshire in the region of the Bronson Hill anticlinorium (after Billings, 1937, and Moench, 1989). The regional location is indicated in the inset showing the approximate locations of the Connecticut Trough (CT), the Bronson Hill anticlinorium (BHA), and the Kearsarge-Central Maine syncline (KCMS). Additional structures indicated on the main figure include the Ammonoosuc Fault (AF), the Salmon Hole Brook syncline (SHBS), the Piermont allochthon (PA), and the Moosilauke septum (MS). Identified plutonic bodies include Oliverian gneiss domes (Oo), the Mount Clough Pluton (mcp), the Haverhill Pluton (hp), and stocks of the New Hampshire Plutonic Series (Dnh).

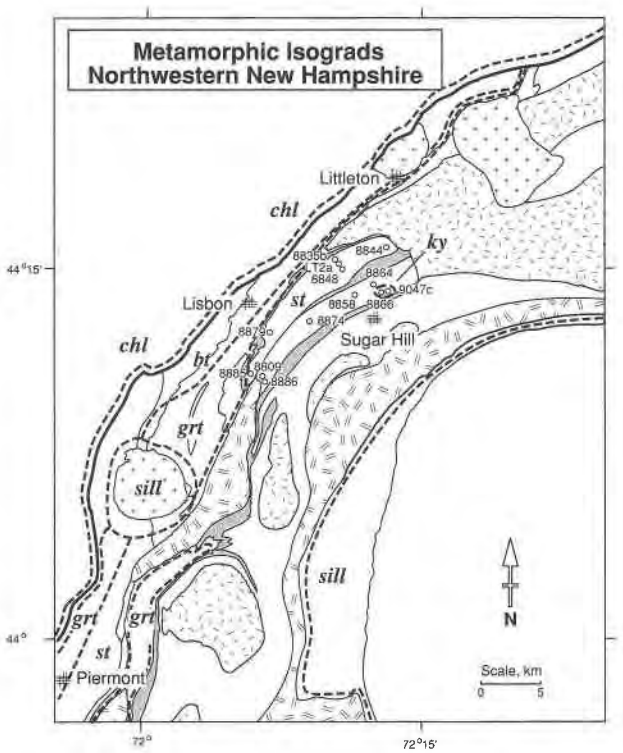

Fig. 2. Simplified geologic map showing sample locations in the Salmon Hole Brook syncline and the position of metamorphic isograds on both flanks of the Bronson Hill anticlinorium in northwestern New Hampshire. Note the general pattern of increasing grade eastward from the Ammonoosuc Fault, and the contact aureole surrounding the French Pond intrusion. Abbreviations: chl = chlorite, bt = biotite, grt = garnet, st = staurolite, ky = kyanite, and sill = sillimanite.

silicate triple point of Holdaway (1971) is indicated, based on the calculated *P-T* conditions of this sample.

Pressure and temperature estimates

Figure 2 shows the distribution of samples across the Salmon Hole Brook syncline used to determine the pressures and temperatures of equilibration, and calculated *P-T* conditions are presented in Figure 3 and Table 1. Thermobarometry was based on the garnet-plagioclase-muscovite-biotite net-transfer reaction as calibrated by Hodges and Crowley (1985), the garnet-plagioclase-kyanite-quartz net-transfer reaction as calibrated by Koziol (1989), and the Fe-Mg exchange between garnet and biotite as experimentally determined by Ferry and Spear (1978), corrected for mixing in garnet as modeled by Berman (1990). The imprecision listed with each determination represents uncertainties associated with microprobe analyses and the uncertainty associated with different choices of mineral pairs. Geothermometry calculations were based on minimum Fe/(Fe + Mg) ratios near garnet rims and the composition of matrix biotite not in contact with the garnet. These temperatures are thus minimum estimates of the highest temperatures of metamorphism and underestimate the actual peak conditions in samples with retrograde modification of garnet rim compositions. Geobarometry calculations were based on garnet compositions coincident with the Fe/(Fe + Mg) minimum, rim compositions of matrix plagioclase, and matrix biotite and muscovite.

There is considerable spread in the results obtained from Littleton Formation samples. The median values for the temperature estimates lie between 510 and 575 °C, and corresponding pressures are between 3.7 and 5.6 kbar. Because the geobarometers have a positive slope, the range in temperature estimates contributes to the calculated range of pressures. In fact, the range in median positions of the K_{eq} curves of the geobarometers is less than 1.3 kbar. With the exception of two samples from the southern terminus of the syncline (8885 and 8886), median K_{eq} lines for the Littleton Formation samples all pass through the stability field of kyanite in the temper-

ature range of 450–600 °C, consistent with the presence of kyanite in some samples.

Two lines of reasoning suggest that the range in calculated temperatures does not reflect actual differences in conditions of metamorphism. First, these temperatures differ from the thermal progression expected for a prograde metapelitic paragenesis, i.e., increasing temperatures from staurolite grade to kyanite grade. Second, there is no systematic spatial arrangement of higher or lower *P-T* estimates in the area studied. In some cases, temperature estimates from samples collected along continuous or closely spaced exposures of outcrop differ by more than 50 °C. Possible causes for the range of temperature estimates might include (1) localized or nonsynchronous attainment of equilibrium or disequilibrium; (2) differences in bulk composition or f_{O_2}; or (3) modification of element partitioning by diffusion or reaction history. Each of these concerns is considered below.

1. Episodic metamorphic events are not indicated on the basis of *P-T* paths or mineral textures. The widespread occurrence of postkinematic staurolite reveals that prograde metamorphism continued after the dominant phase of deformation had ceased. *P-T* path models reflect a consistent thermotectonic evolution (Florence, 1991). Partitioning of Fe and Mg among biotite, chlorite, and staurolite was observed to be systematic, a result that is inconsistent with gross chemical disequilibrium.

2. There is no evidence that Fe-Mg partitioning reflects variation in f_{O_2}. All samples contain graphite in the matrix, and it is commonly found as inclusions in garnet. No samples contain magnetite or epidote, and ilmenite is common in all of them. The Fe^{3+} content of biotite in these samples is therefore estimated to be too low (see Dyar, 1989) for any variation to strongly modify the spread in geothermometry estimates. Although there is some variation in bulk composition among the samples, the compositional variation is not sufficiently large that the range of temperature estimates is thought to reflect errors in nonideal mixing corrections in the geothermometer.

3. Estimated temperatures appear to be strongly correlated with mineral assemblages, as indicated in Figure 3. Although there is a small range of overlap in temperature determinations from different assemblages, there is a consistent relationship between peak temperature estimates and mineral assemblage. Kyanite + staurolite + garnet + biotite assemblages give temperatures that are on the order of 15 °C lower than those deduced from garnet + biotite + chlorite, and staurolite + garnet + biotite + chlorite assemblages have temperatures that are 30–60 °C lower than those deduced from garnet + biotite + chlorite assemblages. The apparent range in associated pressures suggests that the temperature estimates fail to represent an array of peak conditions. If the calculated temperatures were accepted uncritically, the variation in pressures would suggest that there was a vertical separation of more than 3 km between samples now found within a few hundred meters of each other (e.g., samples 8835b and 8848.)

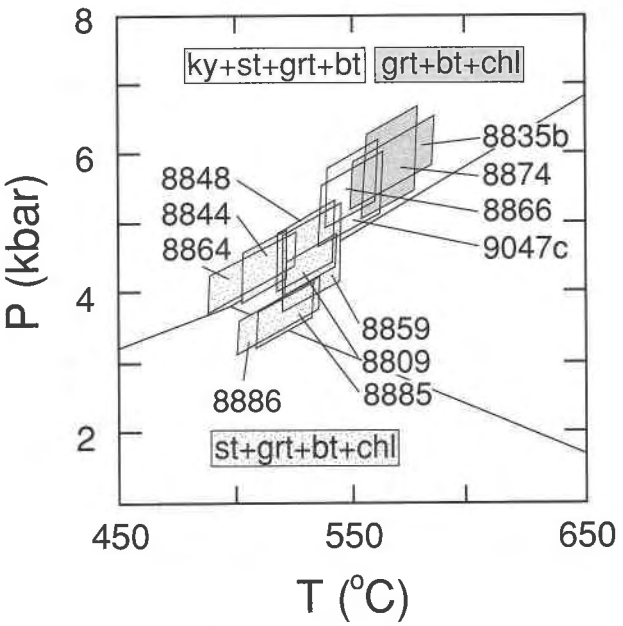

Fig. 3. Pressure-temperature plot showing the estimated conditions of equilibration from Littleton Formation samples. The range of estimates for all staurolite + garnet + biotite + chlorite assemblages lies below about 550 °C, whereas staurolite + garnet + biotite + kyanite and garnet + biotite + chlorite assemblages (shaded) record temperatures to as high as 585 °C.

Consequence of mineral reactions and diffusion

The correlation of lower *P-T* estimates with staurolite + garnet + biotite + chlorite assemblages suggests a cause related to reaction history. This finding is consistent with the consequences of staurolite production as described by Spear et al. (1990) and Spear (1991) on the basis of thermodynamic modeling. Their analysis in the KNaCaMnFMASH system predicts that, for a system closed to all components except H_2O and material fractionated into garnet, staurolite, and biotite, production proceeds at the expense of garnet and chlorite. Continued crystallization of staurolite leads to decreasing molar abundance of garnet, with the extent of garnet resorption proportional to the abundance of chlorite. The loss of compositional zoning from garnet has important implications for *P-T* calculations. Progressive consumption of garnet will move the grain boundary inward, and there is the likelihood that inappropriate ratio of Fe and Mg in garnet will be used in thermometry calculations. For pelitic garnets grown over a heating path, this will lead to temperature estimates lower than true peak temperatures. Furthermore, cation diffusivities are sufficiently rapid at amphibolite grade and during subsequent cooling to partially relax compositional gradients in garnet and induce

retrograde zoning profiles at grain rims. As a result, Fe/(Fe + Mg) ratios near the garnet rim are displaced to higher values, which will also tend to shift geothermometry calculations to lower temperatures.

Retrograde formation of chlorite due to breakdown of garnet can also remove zoning information from the rim of garnet. As above, this may mean that the Fe/Mg ratio in garnet used in thermometry will not reflect maximum thermal conditions. This reaction may also shift biotite to more Fe-rich compositions, introducing further imprecision into geothermometry estimates.

Description of forward models

In order to assess quantitatively the extent that garnet-consuming reactions and intracrystalline diffusion might have affected thermobarometry calculations from the Littleton Formation, the heating and cooling histories of different mineral assemblages were simulated employing numerical models of net-transfer and exchange reactions in combination with estimates of intracrystalline diffusion in garnet. These forward models also allowed evaluation of the internal consistency of various parameters used to develop a petrological interpretation for the samples, including *P-T* paths and temperature-time evolution.

The simulations involved iterative calculations between two computational modules. In the first module, mineral growth and reaction were simulated in the KNaCaMnFMASH system using the Gibbs method, following the procedure detailed in Spear (1988). This is a local equilibrium model that incorporates thermodynamic and mass balance constraints in a system of equations that has two degrees of freedom for closed systems, or 2 + i degrees of freedom, in a system open to i components. Variables that can be considered include pressure, temperature, modal abundances, compositions of solid-solution phases, and molar abundances of system components. A fractional crystallization growth model for garnet was assumed, resulting in development of compositional zoning profiles. Homogeneous equilibrium was assumed in all other phases. Thermodynamic data for minerals were taken from the internally consistent thermodynamic data base of Berman (1988), and the equation of state for H_2O was adopted from Haar et al. (1979). Solid-solution behavior for multicomponent phases was modeled as ideal. The second numerical module consists of a finite-difference algorithm that calculates the effects of quaternary intracrystalline diffusion in garnet (Florence and Spear, 1991). This permits estimation of relaxation of growth zoning profiles due to diffusion and provides a quantitative measure of the flux of components across the garnet rim for each time step. The tracer diffusivities for garnet reported in Loomis et al. (1985) were combined with the model of Lasaga (1979) to calculate a multicomponent diffusion coefficient matrix appropriate for each compositional increment in these calculations. Precision in the finite difference routine was found to be maintained by restricting incremental heating and cooling step sizes to between 0.25 and 1.0 °C.

Prescribed initial conditions for the simulations included the mineral assemblage, modes, and *P-T* conditions assumed for the time of garnet nucleation, as well as garnet nucleation density. Garnet composition in the input model assemblages was set equal to the measured garnet core composition, and the starting matrix assemblage consisted of biotite, chlorite, plagioclase, muscovite, quartz, and H_2O in partitioning equilibrium with garnet, as determined from phase equilibria. A nucleation density per 100 cm^3 of rock for garnet was specified at the start of a simulation that yielded a crystal size at the end of the trial typical of garnet grain sizes in the actual samples. Input parameters included the *P-T* path, heating and cooling rates, cation diffusivities in garnet, and a reaction history for each assemblage consistent with petrographic evidence. Estimation of the temperature for the nucleation of staurolite was based on the KFMASH system petrogenetic grid of Spear and Cheney (1989), which predicts that the garnet + chlorite = staurolite + biotite univariant reaction will occur at a temperature of 564 °C and a pressure of 5 kbar. Spear and Cheney also calculated the extent to which the addition of MnO acts to stabilize garnet + chlorite assemblages to higher temperatures. A linear approximation of their results suggests that the temperature of staurolite nucleation is shifted upward 0.9 °C for each 0.01 increase in the mole fraction of spessartine. Accordingly, temperatures of 564–568 °C were assumed for nucleation of staurolite, corresponding to garnet rim X_{Sps} (where X_{Sps} is defined as the mole fraction of spessartine in a quaternary garnet) in the range 0.002–0.039.

A *T-t* history was used in each simulation that was consistent with the geochronological data. Garnet growth is assumed to have continued to about the time of peak thermal conditions, suggesting that crystallization took place between 410 and 390 Ma. The actual time of garnet crystallization may have been only a portion of this period, as indicated from other regional metamorphic terranes (Christensen et al., 1989; Vance and O'Nions, 1990), therefore a growth rate corresponding to a heating rate of 25 °C/m.y. was initially assumed in all simulations. This resulted in growth times of between 1.24 and 4.6 m.y. for the different cases. Establishing the cooling rate for this region required estimation of the closure temperature for Ar diffusion from hornblende, itself a function of the cooling rate. Calculations were made using the closure ages for hornblendes in northern New Hampshire (Spear and Harrison, 1989), assuming spherical diffusion domains in hornblende with a radius of 50 ± 10 μm and cooling from peak temperatures of 565 ± 20 °C. Diffusion data for Ar were taken from Harrison (1981). On the basis of these parameters, post-Acadian cooling is indicated to have proceeded at an averaged rate between 1 and 3 °C/m.y. However, there is no a priori reason to assume a linear cooling rate for these rocks, and the cool-

ing rate was treated as a free parameter in the simulations. This point is reevaluated below.

Success of an individual simulation was determined by the ability to replicate mineral compositions and modes, mineral zoning in garnet, and the maximum observed size of garnet grains. Although the large number of variables that can be adjusted in these forward models precludes arguing for the uniqueness of any successful simulation, in application it was found that the acceptable range for assumed *P-T* conditions of nucleation and for heating and cooling rates was small, typically less than a few degrees.

Results of forward models

Three assemblages were modeled: (1) staurolite + garnet + biotite + chlorite, (2) kyanite + staurolite + garnet + biotite, and (3) garnet + biotite + chlorite. The results were then used to appraise assumptions regarding estimated peak temperature and pressure conditions, cooling rates, and *P-T* path reconstructions based on mineral compositions. Even though any one of these simulations does not constitute a unique representation of prograde and retrograde reaction history, when all are considered together, they form a cogent model of the *P-T*-reaction paths for these samples. By considering the results obtained from simulated reaction histories of these assemblages, one can gain useful insights bearing on the actual array of peak temperatures.

Case 1: Staurolite + garnet + biotite + chlorite assemblage. Sample 8864 is from a graphitic schist and contains the assemblage staurolite + garnet + biotite + chlorite in a matrix of quartz, muscovite, plagioclase, and ilmenite. Two biotite habits were recognized: small grains up to 0.2 mm in length are aligned with the matrix foliation, and biotite porphyroblasts up to 2.0 mm in length are abundant and randomly disposed with regard to the foliation. Many of the biotite porphyroblasts have sigmoidal trails of quartz and graphite inclusions in their cores and clear rims (Fig. 4a). Concentrations of biotite grains formed around garnet rims locally. Small grains of chlorite are intermixed with the micaceous foliation, and a few porphyroblastic laths crosscut foliation. All chlorite grains are compositionally uniform within the resolution of the electron microprobe. Plagioclase is generally xenoblastic and typically preserves a zoning trend of decreasing anorthite towards the rim, from 0.33 to 0.30. Staurolite porphyroblasts are randomly oriented with respect to the foliation and are moderately to highly poikiloblastic. The great majority of inclusions are quartz, but a few garnet crystals are also included in staurolite. The ZnO content in staurolite ranges from 0.10 to 0.42 wt%.

Garnet porphyroblasts preserve features suggesting that their growth was pre- to syndeformational. Micaceous foliation is flattened around garnet grains, and there are crenulations in adjacent pressure shadows that are truncated against matrix foliation. Many garnets also contain inclusion trails that are sigmoidal and generally at a high angle to matrix schistosity. Garnet morphology is typically close to idioblastic, but intersections of facets around the grain margins have a rounded appearance, suggesting resorption (Fig. 4a). Less commonly, tabular crystals of biotite appear to replace sections of the grain rims inward to 50 μm. Small inclusions of quartz, ilmenite, and chlorite are commonly found within garnets. Chemical zoning in garnets is systematic (Fig. 5): maximum concentration of X_{Sps} occurs at the core and smoothly decreases toward the rim. X_{Grs} is close to uniform or slightly increasing from the core outward for approximately 400 μm, then decreases near the rim. Fe/(Fe + Mg) ratios are nearly flat around the core but decrease appreciably toward the rim. In the outermost 50 μm, there is a reversal in zoning that is most noticeable in the Fe/(Fe + Mg) ratio, which increases by 0.03, and in X_{Prp}, which decreases by a similar magnitude.

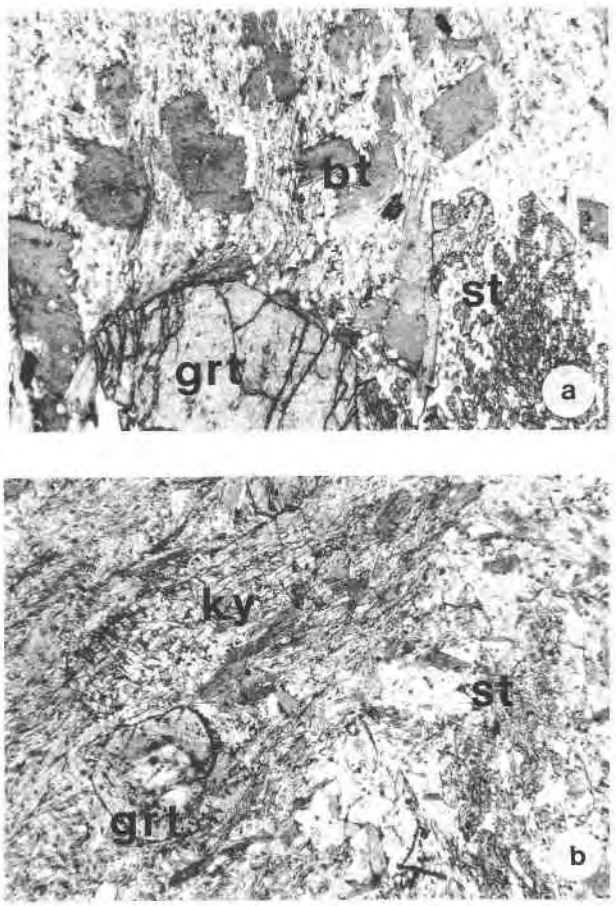

Fig. 4. (**a**) Photomicrograph of sample 8864, showing textural relationships among staurolite (st), garnet (grt), and biotite (bt). Biotite can be seen replacing garnet rims. Also note sigmoidal trails of quartz and graphite that can be seen in the cores of the coarse biotite grains. (**b**) Photomicrograph of sample 8866, showing textural relationships between kyanite (ky), staurolite (st), and garnet (grt). Notice the rounded appearance of the garnet grains. Field of view in each image is 4 mm in width.

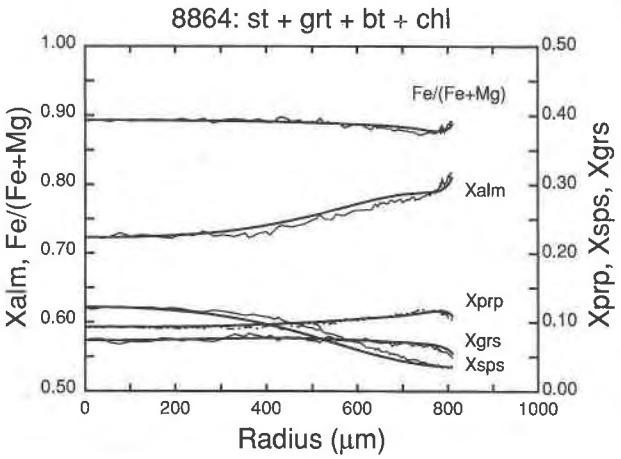

Fig. 5. Measured garnet zoning profiles from sample 8864 (light line) compared with the garnet zoning profile produced during the simulated *P-T-t*-reaction history (heavier line). X_{Prp} is shown as a dashed line for clarity.

Textural relationships, crystal morphology, and inclusion patterns suggest that a single, prograde sequence of reactions is responsible for the observed assemblage. The breakdown of chlorite was likely the dominant reaction responsible for garnet growth. The abundance of grossular in the garnet and the absence of any other calcic phase besides plagioclase indicates that anorthite component was removed from plagioclase as the reaction proceeded. The observed pattern of plagioclase zoning suggests that more albitic plagioclase recrystallized as anorthite was consumed during garnet growth according to the reaction

$$\text{Chl} + \text{Bt} + \text{Pl} + \text{Qtz} = \text{Grt} + \text{Ms} + \text{H}_2\text{O} \quad (1)$$

(mineral abbreviations after Kretz, 1983).

When staurolite entered the assemblage, it grew with biotite at the expense of chlorite, muscovite, and garnet:

$$\text{Grt} + \text{Chl} + \text{Ms} = \text{St} + \text{Bt} + \text{Pl} + \text{Qtz} + \text{H}_2\text{O}. \quad (2)$$

Forward models of the growth and cooling history of this sample were constructed based on the compositional and petrographic information. Starting *P-T* conditions for the most successful simulation are summarized in Table 2, and the input *P-T* and *T-t* trajectories are shown in Figure 6. Starting volume percent of chlorite was calculated from the combined modal proportion of chlorite, garnet, and staurolite. Growth and compositional evolution for the garnet + biotite + muscovite + chlorite + plagioclase + quartz + H_2O assemblage were calculated along the assumed *P-T-t* path up to a temperature of 564 °C. At this point, staurolite in Mg-Fe-Mn partitioning equilibrium was added to the assemblage, then allowed to grow along the input *P-T* path. Staurolite crystallization was assumed to proceed until the volume percent of chlorite was reduced to 0.10 ($\Delta T = 1.3$ °C). Garnet radius decreased in this interval by 27%, and the equilibrium Fe/(Fe + Mg) at the garnet rim decreased by about 1.5%.

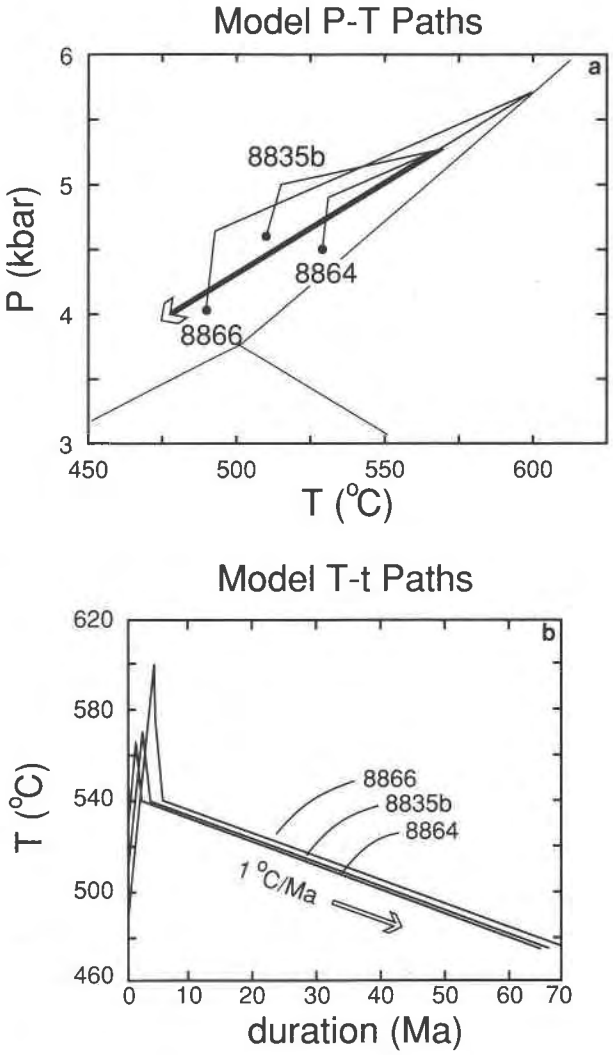

Fig. 6. (**a**) Pressure-temperature diagram showing the *P-T* paths for the simulated growth and reaction histories of the model assemblages that best fit all compositional constraints. (**b**) Temperature-time diagram showing the heating and cooling rates for the same simulations.

However, as no new garnet material of this composition was added to the grain, a nearly infinite compositional gradient was imposed at the rim. H_2O was then removed from the model assemblage to block hydration net-transfer reactions along the cooling path. The assumed equilibrating assemblage was then cooled to 475 °C.

A series of tests was conducted assuming linear cooling rates between 0.5 and 10 °C/m.y., but none yielded successful matches to the observed zoning trends in garnets. Faster cooling rates tended to provide the best matches to the zoning curvatures in the core region of the garnet but failed to replicate the zoning reversals near the rims. A cooling rate of 1 °C/m.y. successfully matched the rim profiles but led to undesirable relaxation in zoning curvatures, particularly in X_{Alm} and X_{Sps}. A substantially improved match was obtained by assuming a two-stage

cooling model involving initial rapid cooling to 540 °C at 25 °C/m.y., followed by slow cooling at 1 °C/m.y. to 475 °C (Fig. 6). This corresponds to a total cooling history of 66 m.y., which is consistent with the known geochronology of the region.

The results of the simulation are compared with the measured zoning profiles in Figure 5. Model garnet rim compositions and zoning trends were modified by re-equilibration and diffusion during cooling so that, by the end of the simulation, the Fe/(Fe + Mg) profile matched the short increase toward the rim observed in the natural garnet. Volume diffusion produced a minimum Fe/(Fe + Mg) along the simulated profile about 1.0% higher than was present at the peak temperature. As a result, the maximum estimate obtained from garnet-biotite thermometry underestimates the actual peak temperature condition achieved in the simulation (see below). The composition of biotite at the conclusion of the simulation (X_{Ann} = 0.4908) compared reasonably well with the measured composition of the biotite in the sample (X_{Ann} = 0.508). It was observed that the biotite composition remained nearly unchanged during cooling, as expected for a large modal abundance of biotite relative to the mass of equilibrating garnet. The composition of plagioclase decreased by X_{An} = 0.02 during the model history, similar to the recognized core to rim decrease in the sample.

Case 2: Kyanite + staurolite + garnet + biotite assemblage. Sample 8866 contains kyanite + staurolite + garnet + biotite + plagioclase + muscovite + quartz. In hand sample, it closely resembles the staurolite garnet schist discussed above, but examination in thin section disclosed locally abundant blades of kyanite that are randomly arranged with respect to the matrix foliation (Fig. 4b). Garnet grains have outer margins that are generally more rounded in appearance than in staurolite + garnet + biotite + chlorite assemblages. Porphyroblastic staurolite is abundant and commonly encloses garnet grains. Margins of staurolite grains are irregular, and because of their highly poikiloblastic nature it is difficult to assess whether their textures indicate resorption. A crenulated pattern of quartz inclusions in some staurolite grains preserves evidence of superposed deformation regimes. The later deformation is also recognized in the matrix, where it has developed into a tight crenulation cleavage predominantly made up of muscovite and quartz, with some aligned grains of biotite. There is also abundant porphyroblastic biotite that has overgrown the crenulation. There is no chlorite in the matrix, although it is present as inclusions in garnet, supporting the assumption that garnet growth prior to the formation of staurolite was due to the continuous reaction of chlorite.

The kyanite staurolite schists are among the most Mn-rich rocks recognized in the study area, as shown by the high spessartine content of the garnets (Table 1), and all mineral compositions have relatively low Fe/(Fe + Mg). In this bulk composition, kyanite may have entered the assemblage soon after the nucleation of staurolite as a result of the AFM reaction

TABLE 2. Calculated *P-T* conditions

Sample	Assemblage	*P* (bars)	*T* (°C)
8835b	Grt + Pl + Bt + Ms + Chl	5800 ± 600	565 ± 25
8864	St + Grt + Pl + Bt + Ms + Chl	4300 ± 600	510 ± 25
8866	Ky + St + Grt + Pl + Bt + Ms	5500 ± 600	550 ± 25

$$St + Chl + Ms + Qtz = Ky + Bt + H_2O. \quad (3)$$

The assemblage kyanite + staurolite + biotite indicates a shift in intensive parameters from conditions that produced the staurolite + garnet + biotite + chlorite assemblage. However, quantifying the shift is made complicated by retrograde adjustments to the mineral compositions in both assemblages. Production of garnet by the kyanite-forming reaction is suggested petrographically: portions of the rims of garnets have thin regions (≈10 μm) containing a stepped pattern of narrow, parallel facets. This texture was not observed in either garnet- or staurolite-grade rocks, and it is interpreted to be new garnet grown with kyanite according to the reaction

$$St + Pl + Ms + Qtz = Ky + Grt + Bt + H_2O. \quad (4)$$

Presumably this reaction began after chlorite was consumed during staurolite production.

Simulation of the reaction history of this assemblage was made following the procedure outlined above, and initial conditions are presented in Tables 2 and 3. The simulation assumed garnet growth began at 490 °C and 4000 bars and continued to 568 °C and 5350 bars, at which point X_{Sps} was equal to 0.039. Staurolite was then introduced to the assemblage and allowed to crystallize during continued heating. Chlorite was eliminated in all simulations within 5 °C of heating from the first appearance of staurolite. Tests were conducted that assumed nucleation of kyanite by means of Reaction 3 at temperatures between 568 and 573 °C, that is, at temperatures nearly identical to the maximum conditions indicated by simulations of the staurolite + garnet + biotite + chlorite assemblage. However, results from these tests significantly underestimated the observed decrease in the Fe/(Fe + Mg) profile in the sample. A better match was obtained by assuming that kyanite was produced by Reaction 4, but only after considerable heating above conditions of staurolite nucleation. In the most successful simulation, Reaction 2 was allowed to proceed until chlorite abundance was less than 0.001, at which point the phase was eliminated from the assemblage. Heating was continued to 599 °C, where kyanite was added to the assemblage. Kyanite growth was modeled to reproduce the 2% modal abundances observed in thin section and involved the consumption of 10% of the volume of staurolite over a calculated 2.0 °C increment. Growth of kyanite resulted in a perceptible radial increase in garnet (10 μm), in agreement with the petrographic evidence from Salmon Hole Brook syncline samples.

TABLE 3. Input conditions for growth simulations

Model no.		8835b	8864	8866
Starting *P-T* conditions		510 °C 4600 bars	529 °C 4500 bars	490 °C 4000 bars
Mineral compositions:				
Quartz	X_{Qtz}	1.0000	1.0000	1.0000
Muscovite	X_{Ms}	1.0000	1.0000	1.0000
Biotite	X_{Phl}	0.3450	0.4512	0.4311
	X_{Ann}	0.6503	0.5458	0.5558
	$X_{Mn\text{-}Bt}$	0.0047	0.0030	0.0132
Chlorite	X_{Cln}	0.3685	0.4758	0.4532
	X_{Dph}	0.6250	0.5193	0.5250
	$X_{Mn\text{-}Chl}$	0.0066	0.0049	0.0218
Plagioclase	X_{Ab}	0.6600	0.6700	0.6100
	X_{An}	0.3400	0.3300	0.3900
Garnet	X_{Prp}	0.0536	0.0900	0.0500
	X_{Alm}	0.7005	0.7110	0.4800
	X_{Sps}	0.1359	0.1280	0.3300
	X_{Grs}	0.1100	0.0710	0.1400
H_2O	X_{H_2O}	1.0000	1.0000	1.0000
Modal proportions:				
Quartz		35.0	25.0	20.0
Muscovite		24.9	25.0	10.0
Biotite		21.0	19.0	15.0
Chlorite		4.1	21.0	45.0
Plagioclase		15.0	10.0	10.0
Garnet		0.0	0.0	0.0
H_2O		0.0	0.0	0.0
Garnet nucleation density (per 100 cm³)		2000	700	5000

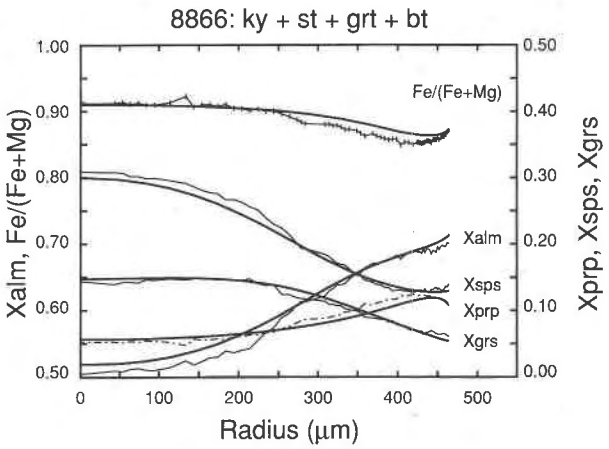

Fig. 7. Measured garnet zoning profiles from sample 8866 (light line) compared with the garnet zoning profile produced during the simulated *P-T-t*-reaction history (heavier line).

Cooling effects were calculated to a final temperature of 475 °C, assuming either linear or multistage cooling rates. As for Case 1, those models that assumed linear cooling rates of 1–5 °C/m.y. failed to provide acceptable matches to measured garnet profiles. Fits were demonstrably improved by assuming that initial rapid cooling was followed by slow cooling to a closure temperature. The most satisfactory fit assumed that cooling progressed at 50 °C/m.y. from the peak temperature to 575 °C, then at 25 °C/m.y. to 540 °C, and finally at 1 °C/m.y. to 475 °C.

The final garnet zoning profile as calculated is compared with the measured profile in Figure 7. The slight increase in X_{Grs} from the core outward for about 200 μm observed in the sample was successfully simulated by assuming a steep initial dP/dT slope, and the model path reproduced the general features of all garnet zoning trends, although some discrepancies are recognizable. For example, diffusional homogenization has led to low abundances of X_{Sps} and X_{Alm} in the core. This may reflect excessive calculated diffusion effects in the simulation or may imply that the garnet compositions in the sample core experienced partial diffusional homogenization since the time of nucleation. In the outer 200 μm of the profile the simulation curves reflect the general zoning trends of the sample but fail to replicate details. Encouragingly, the rim composition for the simulated garnet is within 0.01 of the measured values of the mole fraction of each component. Biotite composition in the simulation is X_{Ann} = 0.452, compared with 0.46 in the sample. Plagioclase composition is calculated at X_{An} = 0.301, in good agreement with the measured sample composition (0.31).

Case 3: Garnet + biotite + chlorite assemblage. Sample 8835b contains the assemblage garnet + biotite + chlorite + plagioclase + muscovite + quartz + ilmenite. Garnet textures suggest that its growth was at least in part syndeformational: crystals contain sigmoidal inclusion trails of ilmenite, and orientation of inclusion trails varies among grains. A weak crenulation cleavage is preserved in strain shadows around the garnets but is absent elsewhere. Inclusion abundance decreases near the rims, and grains display sharply faceted margins. Plagioclase and biotite are abundant, but chlorite is much less common. Chlorite formed adjacent to garnet rims, as replacement for some biotite, and as matrix grains that crosscut foliation. These textures suggest that all chlorite now in the sample formed during retrograde metamorphism.

Garnets exhibit compositional zoning in all components. Both X_{Sps} and X_{Grs} decrease from core to rim, while both X_{Alm} and X_{Prp} increase outward (Fig. 8). Plagioclase grains are zoned from X_{An} to 0.39 and 0.42 in the core to X_{An} = 0.28–0.30 at the rims.

Starting conditions for the numerical simulation of garnet growth in this sample are summarized in Tables 2 and 3. A mass balance calculation was made to convert the present modal proportion of garnet to the equivalent volume percent of chlorite that would have been present at the time of garnet nucleation. In the simulation, garnet growth was calculated up to 553 °C, by which temperature all chlorite was consumed. Chlorite was then subtracted from the model assemblage, and the simulation was continued through additional heating to the assumed thermal maximum. Cooling effects were calculated to 475 °C.

Constant cooling rates between −1 and −10 °C/m.y. were tested and evaluated against the actual garnet zoning profiles for goodness of fit, but all failed to provide close

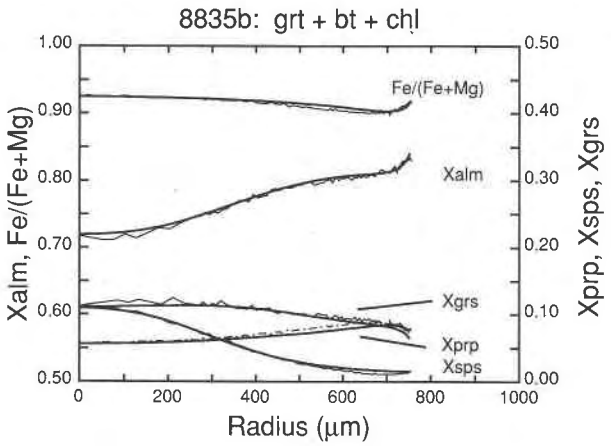

Fig. 8. Measured garnet zoning profiles from sample 8835b (light line) compared with the garnet zoning profile produced during the simulated *P-T-t*-reaction history (heavier line).

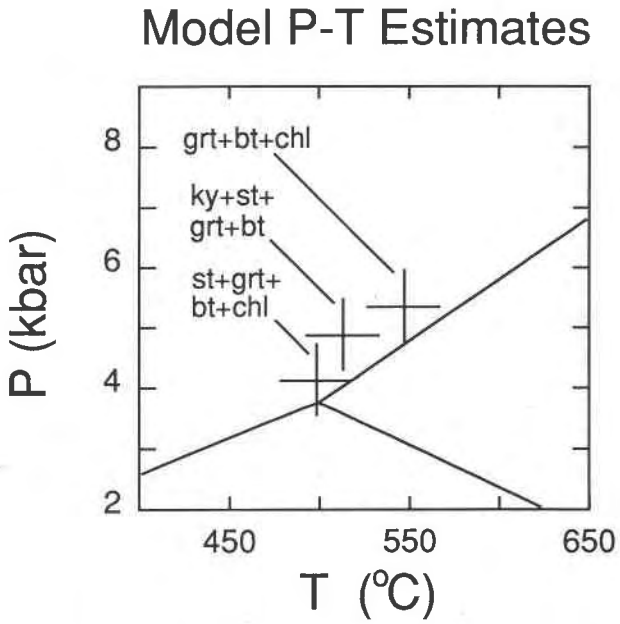

Fig. 9. Thermobarometry estimates based on garnet-biotite $FeMg_{-1}$ exchange and garnet + plagioclase + biotite + muscovite equilibria using garnet compositions at the end of the cooling portion of each simulation and the equilibrium composition of matrix biotite and plagioclase.

matches to the measured zoning curvature. An acceptable match was obtained when the cooling rate was assumed to be 25 °C/m.y. from the peak temperature to 540 °C, followed by cooling at a rate of 1 °C/m.y. to the final temperature of 475 °C. Figure 8 shows a comparison of the measured garnet zoning profiles from sample 8835b and the profiles obtained at the conclusion of the simulation. Overall, there is a very good match of the curvatures of the various compositional trends, and mole fractions of all model components are within 1% of measured values.

The high calculated temperatures from the sample reflect the higher annite component in the natural biotite (X_{Ann} = 0.617). However, consideration of the results of the simulation indicate that it is unlikely that the biotite composition of the sample was in equilibrium with garnet at the peak temperature. Because of the large modal ratio of biotite to garnet, biotite is not expected to have significantly shifted composition if only exchange reactions operated during cooling. However, when the composition of the model garnet at the peak temperature is used in combination with the measured composition of biotite, one obtains a geothermometry estimate of approximately 650 °C, well above the simulation maximum temperature and suggesting that some important aspect of the reaction history has been overlooked.

The presence of retrograde chlorite in the sample implies that a hydration event occurred during cooling. A chlorite-producing hydration of the form

$$\text{Grt} + \text{H}_2\text{O} = \text{Chl} + \text{Qtz} \qquad (5)$$

causes a shift of the entire garnet + chlorite + biotite assemblage to more Fe-rich compositions as the reaction proceeds, producing a more Fe-rich biotite through exchange equilibrium even though biotite does not participate significantly in the hydration reaction. The details of retrograde chlorite formation were explored in a number of simulations. The extent of retrograde hydration (Reaction 5) was monitored by matching the modal abundance of retrograde chlorite produced in the simulation with that observed in the rock. This limited the extent of retrograde hydration to occur over a 5 °C interval, which was taken to be between 550 and 545 °C. H_2O was removed from the assemblage, as might be the case for a transient hydration episode. The resulting assemblage was cooled to a closure temperature of 475 °C, at which point X_{Ann} in biotite was 0.6086, in very good agreement with the measured value.

Discussion

Evaluating petrological calculations through use of forward modeling

The foregoing simulations permit evaluation of the significance of thermometry, *P-T* path calculations, and assumptions regarding cooling rates for the Salmon Hole Brook syncline samples. Temperature and pressure calculations using compositional information from the conclusion of each simulation are presented in Figure 9. In calculating these *P-T* estimates, petrologic assumptions were made regarding the treatment of the final compositions near the garnet rim in the models. Following the same approach as for the natural samples, garnet compositions at the minima in Fe/(Fe + Mg) and X_{Grs} were used for thermobarometry, along with the compositions of matrix biotite and plagioclase. The lowest temperature estimates were obtained from the Case 1 simulation, in which staurolite production involved the consumption of

garnet rim material. In the trial that gave the best match to modal and compositional constraints, the maximum recovered temperature from garnet-biotite thermometry was 498 °C, which underestimates the maximum temperature of the simulation by 66 °C. The preferred simulation for the assemblage containing kyanite yielded a calculated thermal maximum 16 °C higher than the staurolite + garnet + biotite + chlorite model, but which underestimated the maximum temperature of the simulation by 86 °C. Growth of new garnet rim material by Reaction 4 would modify the extent of diffusional reequilibration in the garnet, and this may account for kyanite assemblages retaining higher temperature compositions. Despite effects of diffusional reequilibration in garnet, the calculated maximum temperature from the garnet + biotite + chlorite model assemblage is 39 °C greater than for the kyanite-bearing assemblage and only underestimates the maximum conditions of the simulation by 22 °C, as a result of retrograde modification to biotite.

These results show a strong resemblance to the temperature estimates obtained from the Salmon Hole Brook syncline (Fig. 3). All the examined assemblages appear to have been metamorphosed to lower amphibolite facies conditions, yet the highest temperatures are recorded in garnet + biotite + chlorite assemblages. Staurolite schists consistently preserve lower temperature estimates until kyanite enters the assemblage. Even then, temperature estimates fall below those predicted in petrogenetic grids constructed from internally consistent thermodynamic data bases for the formation of kyanite by either Reaction 3 or Reaction 4 (e.g., Spear and Cheney, 1989, >605 °C; Powell and Holland, 1990, >625 °C). None of the geothermometry estimates from the field samples indicate that temperatures of metamorphism were this high. Although it is likely that the positions of the reaction curves on these KFMASH grids are higher than those realized in natural rocks, the simulations demonstrate the feasibility that retrograde reactions operating during slow cooling have thoroughly modified mineral K_d values so that peak temperatures that approach 600 °C cannot be recovered. This conclusion is supported by the observation that in all the staurolite-bearing samples there are compositional reversals near garnet rims indicating diffusional reequilibration.

Garnet consumption in staurolite + garnet + biotite + chlorite assemblages can also make obtaining accurate pressure estimates from these rocks problematic. Beginning at the staurolite isograd, X_{Grs} increases with increasing temperature, but this may not be recognized because garnet tends to be resorbed back to higher X_{Grs} concentrations as staurolite grows. This has the effect of minimizing the error introduced by treating near-rim compositions as if they actually were the equilibrium composition for conditions above the staurolite isograd. Nonetheless, this error may result in overly high pressure estimates because of the sensitivity of geobarometry on grossular content. For example, for the compositional range of the Littleton rocks, dP/dX_{Grs} is between 700 and 3000 bars/mol% using garnet-plagioclase-biotite-muscovite geobarometry.

Plagioclase will grow as garnet is consumed along heating trajectories, but the increase in its abundance may be <1 modal% across the staurolite isograd. The sensitivity of pressure estimates to plagioclase compositions is less than for garnet: calculations for the Littleton Formation metapelites indicate that dP/dX_{An} is between 125 and 450 bars/mol%. Overly high pressure estimates will be obtained if the equilibrium garnet rim composition is used in geobarometry, but this new plagioclase composition is overlooked. Other incorrect combinations are imaginable. An immediate benefit of having the predictive model for petrological studies is that it emphasizes the need to explore thoroughly for both discontinuities in garnet and compositional trends in plagioclase.

In every case, the most acceptable simulations involved *P-T* trajectories with steep dP/dT slopes during the early growth of garnet. Pressure increases were between 400 bars over 5 °C for model 8835b and 600 bars in 3 °C for model 8866. Subsequent heating involved continued pressure increases in all models. The consistency of these results supports the increasing pressure trajectories calculated for the Salmon Hole Brook rocks on the basis of mineral growth zoning and suggests that Gibbs method path calculations can be made to infer useful thermobaric information from staurolite-grade metapelites.

A notable result of these simulations was the failure of linear cooling rates to provide acceptable matches to the compositional constraints, particularly the curvature in the garnet zoning profiles. On the other hand, the successful two- and three-stage cooling histories are fully consistent with the available geochronological data and suggest that alternative interpretations be considered regarding the thermal conditions during metamorphism. For example, bipartite cooling paths (or broadly comparable exponential cooling paths) might be the result of rapid unroofing, followed by slower thermal relaxation. Alternatively, rapid initial cooling might be a reflection of transient heating associated with syntectonic plutonism. It has been recognized for some time that Acadian metamorphism in central New Hampshire is spatially associated with voluminous granitoid intrusions (Lyons et al., 1982), and similar age intrusions are present in the Bronson Hill anticlinorium. The proximity of the Bethlehem granodiorite to the study area suggests that it may have contributed significantly to the regional thermal budget and that the presence of aluminum silicates in the northwestern portion of the syncline may be an expression of metamorphism that was locally enhanced by contact effects.

Application of reaction model to other terranes

Studies in additional metamorphosed pelitic terranes suggest that anomalous *P-T* estimates may be obtained from samples collected above the staurolite isograd and

emphasize the need to consider thermometry results in the context of potential mineral reactions. Pelitic schists in the Funeral Mountains, southeastern California, show a continuous increase in the conditions of metamorphism from biotite to sillimanite grade (Labotka, 1980). In the staurolite + biotite zone, garnet porphyroblasts show evidence of resorption and are found as inclusions in staurolite. Garnet grains within the kyanite zone, on the other hand, contain inclusions of staurolite and biotite. Temperatures for these samples were calculated from mineral compositions (Labotka, personal communication) using the same thermometry as for the Salmon Hole Brook syncline suite. Results are displayed in Figure 10, where it can be seen that the calculated temperatures show a trend similar to the results from New Hampshire. Temperature estimates from the garnet zone range between about 500 and 600 °C. Staurolite + biotite zone samples yield a narrower range of estimates centered around 505 °C and extend to lower temperatures than those calculated for any garnet zone samples. Kyanite zone rocks give estimates of about 525–635 °C. Although the uncertainties in these estimates are somewhat larger than for the Salmon Hole Brook syncline, it can be seen that the distribution of thermometry estimates fails to match the apparent sequence of increasing metamorphic grade across the staurolite zone. The textural features and paragenetic sequence described by Labotka support the assumption that garnet-consuming reactions are principally responsible for the pattern in temperature estimates.

Treloar et al. (1989) delineated a sequence of metamorphic zones in metapelites in the Hazara region, northern Pakistan. This region experienced imbricate thrusting after the peak of metamorphism that juxtaposed chlorite- through sillimanite-grade rocks. Treloar et al. observed that garnet-biotite thermometry indicated an apparent temperature plateau of about 500 °C in a broad expanse of staurolite-grade rocks. This compares with temperature estimates within the garnet zone of 435–555 °C, and estimates from within the kyanite zone in excess of 550 °C. The authors speculate that unrecognized imbricate thrusts within the staurolite zone might be responsible for the drop in the metamorphic field gradient. Our analysis suggests that the temperatures may be at least partly a result of the prograde reaction responsible for staurolite growth.

Grambling (1991) reported that staurolite schists in northern New Mexico contain garnets in which zoning in Fe/(Fe + Mg) and X_{Sps} increased in the outermost 5–50 μm of the rim. In contrast, similar upturns in the zoning profiles were not observed in garnet + biotite + chlorite assemblages collected from interlayered beds in the same outcrops. Geothermometry estimates from the staurolite schists were 30–40 °C lower than for the staurolite-absent assemblages, which Grambling interpreted as caused by the effects of garnet resorption during staurolite growth.

In contrast, Holdaway et al. (1988) observed a continuous increase in calculated temperatures between garnet and staurolite grades in west-central Maine and inferred

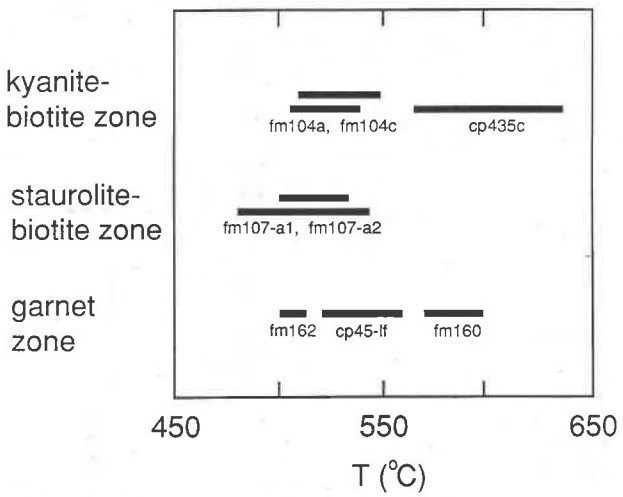

Fig. 10. Temperature estimates for samples in the garnet, staurolite + biotite, and kyanite zones, Funeral Mountains, California (data from Labotka, personal communication). Temperatures were calculated using geothermometry identical to that used on Salmon Hole Brook syncline samples. Although the mineral assemblages define a sequence of increasing metamorphic grade, calculated temperatures do not show a corresponding increasing trend.

continued garnet growth in the staurolite zone by the reaction of staurolite + biotite to garnet + muscovite. Our calculations fail to predict appreciable garnet growth by this reaction, suggesting that our model involves assumptions that are inappropriate for the Maine rocks. Alternatively, models that involve infiltration of K^+ and Na^+ can achieve garnet growth at staurolite grade. Open-system chemical behavior has been postulated for garnet growth in staurolite grade rocks from the Pecos Baldy area of New Mexico (Grambling, 1991). These results emphasize that detailed studies are needed across the staurolite zone to appreciate the controls on mineral compositions intended for use in thermobarometry.

Conclusions

This study details the reaction history and compositional relationships of garnet- and staurolite-grade pelitic schists. It is shown how determination of *P-T* conditions from staurolite-bearing rocks can have a significant uncertainty introduced by both prograde and retrograde reaction history. Duebendorfer and Frost (1988) presented evidence from a metapelite in which retrograde reequilibration and strain-induced dissolution led to a substantial variation in Fe/(Fe + Mg) around the rims of individual garnet crystals. Our study emphasizes that, even in the absence of deformation, prograde mineral reactions and diffusion can induce substantial modification to the measurable composition of garnet rims. Combined reaction and diffusion modeling predicts that temperatures calculated using the Fe-Mg minima preserved in slowly cooled staurolite + garnet + biotite ± chlorite rocks give temperatures that are too low by 40–75 °C. In

the Salmon Hole Brook syncline, garnet consumption associated with staurolite growth has apparently led to the loss of chemical information from garnet, particularly Fe-Mg values representative of the staurolite isograd, as confirmed by the observed pattern of temperature estimates (Fig. 3). The lack of a wide range in the K_{eq} used to estimate pressure is thought to reflect the small size of the compositional modification to X_{Grs} in garnet.

Our analysis leads us to the interpretation that the metamorphism responsible for the mineral paragenesis preserved within the Salmon Hole Brook syncline reflects a single thermotectonic episode. If it is assumed that equilibria reflecting pressure maxima were preserved at temperatures of 565–600 °C in staurolite-grade rocks, then pressures are indicated to have all been between 4.5 and 6.5 kbar across the syncline. The broad uniformity of pressure estimates is consistent with the interpretation, supported by textural evidence, that metamorphism outlasted deformation associated with thrust napping.

Staurolite production, retrograde reaction and intragranular diffusion in garnet make the task of recovering *P-T* conditions from these rocks difficult, emphasizing the need to consider the compositional consequences of mineral reactions when attempting to recover thermobaric conditions of metamorphism. As well, *P-T* path calculations for staurolite grade metapelites that are based on mineral zoning information must take reaction history into account when correlating mineral compositions. Our results demonstrate that an improved understanding of the thermal history of staurolite-grade pelitic rocks can be obtained by considering their phase equilibria in the dynamical context of a pressure-temperature-reaction path. Forward modeling is shown to be helpful in this effort by providing insights into the character of compositional changes that develop as net-transfer reactions and diffusional exchange proceed.

Acknowledgments

T. Labotka kindly provided unpublished compositional data from his study in the Funeral Mountains, California. We thank Jeff Grambling, Mike Holdaway, and John Brady for their constructive reviews. This study has been supported by National Science Foundation research grants EAR-8708609, EAR-8916417, and EAR-8903820 to F.S.S. and Geological Society of America research grant 4195-89 to F.P.F. A Capital District Mineral Club research grant to F.P.F. helped defray costs in fieldwork. We are grateful to all these organizations for their support.

References cited

Albee, A.L., and Ray, L. (1970) Correction factors for electron microanalysis of silicates, oxides, carbonates, phosphates and sulfates. Analytical Chemistry, 42, 1408–1414.

Barreiro, B., and Eusden, J.D., Jr. (1988) Monazite U-Pb ages of schists and migmatites in the Kearsarge-Central Maine synclinorium. Geological Society of America Abstracts with Programs, 20, 4.

Bence, A.E., and Albee, A.L. (1968) Empirical correction factors for the electron microanalysis of silicates and oxides. Journal of Geology, 76, 382–403.

Berman, R.G. (1988) Internally consistent thermodynamic data for minerals in the system Na_2O-K_2O-CaO-MgO-FeO-Fe_2O_3-Al_2O_3-SiO_2-TiO_2-H_2O-CO_2. Journal of Petrology, 29, 445–522.

——(1990) Mixing properties of Ca-Mg-Fe-Mn garnets. American Mineralogist, 75, 328–344.

Billings, M.P. (1937) Regional metamorphism of the Littleton-Moosilauke area, New Hampshire. Geological Society of America Bulletin, 48, 463–566.

Chakraborty, S., and Ganguly, G. (1992) Cation diffusion in aluminosilicate garnets: Experimental determination in spessartine-almandine diffusion couples, evaluation of effective binary diffusion coefficients, and applications. Contributions to Mineralogy and Petrology, 111, 74–86.

Christensen, J.N., Rosenfeld, J.L., and DePaolo, D.J. (1989) Rates of tectonometamorphic processes from rubidium and strontium isotopes in garnet. Science, 244, 1465–1469.

Dickenson, M.P., III (1988) Local and regional differences in the chemical potential of water in amphibolite facies pelitic schists. Journal of Metamorphic Geology, 6, 365–381.

Duebendorfer, E.M., and Frost, B.R. (1988) Retrogressive dissolution of garnet: Effect on garnet-biotite thermometry. Geology, 16, 875–877.

Dyar, M.D. (1989) Mössbauer spectra of biotite from metapelites. American Mineralogist, 75, 656–666.

Ferry, J.M., and Spear, F.S. (1978) Experimental calibration of the partitioning of Fe and Mg between biotite and garnet. Contributions to Mineralogy and Petrology, 66, 113–117.

Florence, F.P. (1991) Diffusional modification of garnet growth zoning and Acadian metamorphism and tectonic history in the Littleton area, northwestern New Hampshire, 205 p. Ph.D. thesis, Rensselaer Polytechnic Institute, Troy, New York.

Florence, F.P., and Spear, F.S. (1991) Effects of diffusional modification of garnet growth zoning on *P-T* path calculations. Contributions to Mineralogy and Petrology, 107, 487–500.

Grambling, J.A. (1991) A problem with garnet thermobarometry in staurolite schist. Geological Society of America Abstracts with Programs, 23, A333.

Haar, L., Gallagher, J., and Kell, G.S. (1979) Thermodynamic properties for fluid water. In J. Straub and K. Sheffler, Eds., Water and steam: Their properties and current industrial applications. Proceedings of the 9th international conference on the properties of steam, p. 69–82. Pergamon, New York.

Harrison, T.M. (1981) Diffusion of ^{40}Ar in hornblende. Contributions to Mineralogy and Petrology, 78, 324–331.

Harrison, T.M., Spear, F.S., and Heizler, M. (1989) Geochronologic studies in central New England. II. Post-Acadian hinged and differential uplift. Geology, 17, 185–189.

Hodges, K.V., and Crowley, P.D. (1985) Error estimation and empirical geothermobarometry for pelitic systems. American Mineralogist, 70, 702–709.

Holdaway, M.J. (1971) Stability of andalusite and the aluminum silicate phase diagram. American Mineralogist, 271, 97–131.

Holdaway, M.J., Dutrow, B.L., and Shore, P. (1986) A model for the crystal chemistry of staurolite. American Mineralogist, 71, 1142–1159.

Holdaway, M.J., Dutrow, B.L., and Hinton, R.W. (1988) Devonian and Carboniferous metamorphism in west-central Maine: The muscovite-almandine geobarometer and the staurolite problem revisited. American Mineralogist, 73, 20–47.

Koziol, A.M. (1989) Recalibration of the garnet-plagioclase-Al_2SiO_5-quartz (GASP) geobarometer and application to natural parageneses (abs.). Eos, 70, 493.

Kretz, R. (1983) Symbols for rock-forming minerals. American Mineralogist, 68, 277–279.

Labotka, T.C. (1980) Petrology of a medium-pressure regional metamorphic terrane, Funeral Mountains, California. American Mineralogist, 65, 670–689.

Lasaga, A.C. (1979) Multicomponent diffusion and exchange in silicates. Geochimica et Cosmochimica Acta, 43, 455–469.

Loomis, T.P., Ganguly, J., and Elphick, S.C. (1985) Experimental determinations of cation diffusivities in aluminosilicate garnets. II. Multicomponent simulation and tracer diffusion coefficients. Contributions to Mineralogy and Petrology, 90, 45–51.

Lyons, J.B., Boudette, E.L., and Aleinikoff, J.N. (1982) The Avalon and Gander zones in central eastern New England. In P. St. Julien and J. Beland, Eds., Major structural zones and faults of the northern Appalachians. Geological Society of Canada Special Paper, 24, 43–66.

Moench, R.H. (1989) Metamorphic stratigraphy and structure of the Connecticut Valley area, Littleton to Piermont, New Hampshire. In J.B. Lyons and W.A. Bothner, Eds., A transect through the New England Appalachians. American Geophysical Union Field Trip Guidebook, T162, 45–52.

Moench, R.H., and Aleinikoff, J.N. (1991) Geologic map of the Littleton-Mousilauke-Piermont area, NH-VT: Type area of the Piermont allochthon: NE–SE. Geological Society of America Abstracts with Programs, 23, 106.

Powell, R., and Holland, T. (1990) Calculated mineral equilibria in the pelite system, KFMASH (K_2O-FeO-MgO-Al_2O_3-SiO_2-H_2O). American Mineralogist, 75, 367–380.

Rumble, D., III (1969) Stratigraphic, structural and petrologic studies in the Mt. Cube area, New Hampshire. Ph.D. thesis, Harvard University, Cambridge, Massachusetts.

Spear, F.S. (1988) The Gibbs method and Duhem's theorem: The quantitative relationships among *P, T,* chemical potential, phase composition and reaction progress in igneous and metamorphic systems. Contributions to Mineralogy and Petrology, 99, 249–256.

——— (1989) Petrologic determination of metamorphic pressure-temperature-time paths. American Geophysical Union Short Course in Geology, 7, 1–55.

——— (1991) On the interpretation of peak metamorphic temperatures in light of garnet diffusion during cooling. Journal of Metamorphic Geology, 9, 379–388.

Spear, F.S., and Cheney, J.T. (1989) A petrogenetic grid for pelitic schists in the system SiO_2-Al_2O_3-FeO-MgO-K_2O-H_2O. Contributions to Mineralogy and Petrology, 101, 149–164.

Spear, F.S., and Harrison, T.M. (1989) Geochronologic studies in central New England. I. Evidence for pre-Acadian metamorphism in eastern Vermont. Geology, 17, 181–184.

Spear, F.S., Kohn, M.J., Florence, F.P., and Menard, T. (1990) A model for garnet and plagioclase growth in pelitic schists: Implications for thermobarometry and *P-T* path determinations. Journal of Metamorphic Geology, 8, 683–696.

Treloar, P.J., Broughton, R.D., Williams, M.P., Coward, M.P., and Windley, B.F. (1989) Deformation, metamorphism and imbrication of the Indian plate, south of the Main Mantle Thrust, north Pakistan. Journal of Metamorphic Geology, 7, 111–125.

Vance, D., and O'Nions, R.K. (1990) Isotopic chronometry of zoned garnets: Growth kinetics and metamorphic histories. Earth and Planetary Science Letters, 97, 227–240.

Manuscript received March 9, 1992
Manuscript accepted November 25, 1992

Appendix 1. Uncertainties in Diffusion Calculations

The precision and accuracy to which diffusivities for garnet components are known at conditions typical of crustal metamorphism introduce further uncertainty into the diffusion calculations. The activation energies, Q, for tracer diffusivities of Mn, Mg, and Fe obtained by Loomis et al. (1985) at 40 kbar are 48, 60, and 61 kcal, respectively, with a reported statistical uncertainty of about 8 kcal each. Chakraborty and Ganguly (1992), on the basis of additional experiments, derived activation energies at comparable pressure of 66, 73, and 71 kcal, respectively, all with uncertainties of about 9 kcal. Florence and Spear (1991) found that, at lower amphibolite facies, uncertainties of about 8 kcal are equivalent to differences in diffusivities arising from temperature variations of ±30–45 °C. In the simulations presented above, which used the data set of Loomis et al. (1985), this statistical uncertainty leads to calculated differences of approximately ±15–20 °C in the apparent peak temperatures shown in Figure 9, although their relative positions remain unchanged. The relative positions also remain nearly the same when the diffusivities reported in Chakraborty and Ganguly (1992) are used, although the predicted retrievable maximum temperature in each case increased by about 25 °C. The most noticeable difference that resulted from using the tracer diffusivities from Chakraborty and Ganguly (1992) data was that, for a given simulation, somewhat less compositional modification was indicated in garnet rims than when calculations were made using the Loomis et al. (1985) data. If cooling rates in the latter portion of the cooling history (<540 °C) were assumed to be slower by a factor of 2, acceptable matches to the measured profiles could be achieved. This would be consistent with the interpretation that cooling took place over a period of time 32.5 m.y. greater than that assumed in the above simulations, yielding total cooling times on the order of 98 m.y. Although this is considerably longer than the times estimated in the previous simulations, these are nonetheless permissible within the uncertainties of the geochronological data. More significantly, no trials using the Chakraborty and Ganguly (1992) data that assumed linear cooling histories provided acceptable matches to the compositional constraints.